European Journal of Pharmaceutics and Biopharmaceutics 200 (2024) 114338

Contents lists available at ScienceDirect

European Journal of Pharmaceutics and Biopharmaceutics

journal homepage: www.elsevier.com/locate/ejpb

Ionizable lipids based on branched fatty acids – An explorative study on Langmuir monolayers

Dorota Pawlowska [a], Nicole Erdmann [b], Manuela Folz [b], Andreas Langner [b], Bodo Dobner [b], Christian Wölk [c,*], Gerald Brezesinski [a]

[a] Max Planck Institute of Colloids and Interfaces, Science Park Potsdam-Golm, Am Mühlenberg 1, 14476 Potsdam, Germany
[b] Martin Luther University (MLU) Halle-Wittenberg, Institute of Pharmacy, Wolfgang-Langenbeck-Straße 4, 06120 Halle (Saale), Germany
[c] Leipzig University, Pharmaceutical Technology, Institute of Pharmacy, Medical Faculty, Eilenburger Strasse 15a, 04317 Leipzig, Germany

ARTICLE INFO

Keywords:
Infrared reflections absorption spectroscopy
Ionizable lipids
Langmuir monolayers
Lipofection
Lipoplex
X-ray scattering

ABSTRACT

Ionizable lipids are a class of pharmaceutical excipients with a main application in lipid nanoparticles for nucleic acid delivery. New ionizable lipids are needed to tune characteristics of lipid-based nucleic acid delivery systems, e.g. stability, nucleic acid loading capacity and binding strength, as well as bio-distribution. Herein, we present the synthesis of three novel ionizable lipids as putative excipients for lipid-based nucleic acid delivery systems. Langmuir monolayer experiments with classical surface pressure/area isotherm evaluation were used to understand the self-assembly behavior of the lipids. Additional experiments with surface sensitive techniques, namely grazing incidence x-ray scattering and infrared reflection–absorption spectroscopy (IRRAS), were performed to understand structural characteristics of lipid associates. The latter technique was also used to investigate the nucleic acid binding process between DNA and the ionizable lipids. Finally, first transfection experiments with the novel lipids formulated as cationic liposomes were performed providing first efficacy data. Although the alkyl chain pattern was comparable for all three ionizable lipids, the results demonstrated that with increasing head-group size the DNA binding capacity changed and the alkyl chain fluidity was increased. The lipid with the lowest phase transition temperature and the smallest packing parameter showed the highest DNA transfer efficiency.

1. Introduction

Since nucleic acids got attention as active pharmaceutical ingredients, e.g. in classical gene therapy [1] or as tool for protein knockdown [2], a new class of pharmaceutical excipients has become prominent: the ionizable lipids. Ionizable lipids are characterized by a basic group which allows a pH dependent switch from the positively charged to uncharged state. Prominent compounds can be found in medicines with marketing authorization: DLin-MC3-DMA (Fig. 1) is the ionizable lipid used in the lipid nanoparticles (LNPs) and responsible for the encapsulation of the therapeutic siRNA in Onpattro® [3]. ALC-0315 and SM-102 are the mRNA complexing ionizable lipids in the LNP formulations of the mRNA-vaccines Comirnaty® and Spikevax®, respectively [4]. Nevertheless, nucleic acid delivery with LNPs is a novel field of drug formulation development, and several questions regarding topics like stability and biodistribution have not yet been fully answered [5–7]. Novel ionizable lipids with systematic structural variations can help to understand lipid based nucleic acid delivery in more detail and, consequently, to improve LNP formulations.

To understand the self-assembly of lipids, Langmuir monolayers are a powerful tool, however, the method is still underestimated. Langmuir monolayer studies, especially when combined with surface sensitive methods for structure investigation or quantification allow understanding the relationship between lipid structural behavior and interaction processes at the lipid interface [8–10]. Langmuir monolayer experiments were used to study the interaction of permanently cationic SAINT lipids with DNA [11,12]. Also for ionizable lipids Langmuir monolayer techniques can be applied to address special questions. With total reflection x-ray fluorescence (TRXF) at lipid monolayers, the protonation degree of the ionizable lipid can be determined [13,14]. Furthermore, infrared reflection–absorption spectroscopy (IRRAS) allows to study interaction of ionizable lipids with nucleic acids resulting also in quantitative information [15–17].

Herein we describe the synthesis of novel ionizable lipids based on

* Corresponding author.
E-mail address: christian.woelk@medizin.uni-leipzig.de (C. Wölk).

https://doi.org/10.1016/j.ejpb.2024.114338
Received 17 March 2024; Received in revised form 19 May 2024; Accepted 21 May 2024
Available online 23 May 2024

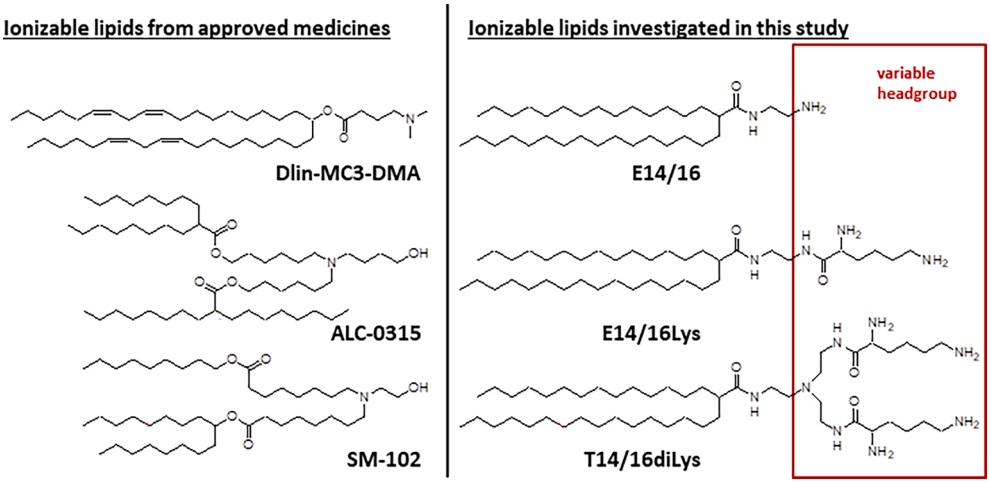

Fig. 1. Left: Structures of ionizable lipids as excipients in approved medicines: Dlin-MC3-DMA (ionizable lipid in Onpattro®), ALC-0315 (ionizable lipid in Comirnaty®), and SM-102 (ionizable lipid in Spikevax®). Right: Structures of 2-tetradecyl octadecanoic acid based ionizable lipids characterized in this study. All three lipids have an ionizable head-group coupled via amide bond. The complexity of the head-group structure increases from **E14/16** < **E14/16Lys** < **T14/16diLys**, resulting in an increasing number of ionizable functionalities: 1 R-NH_2 (**E14/16**) < 2 R-NH_2 (**E14/16Lys**) < 4 R-NH_2 1 R-N-R_2 (**T14/16diLys**).

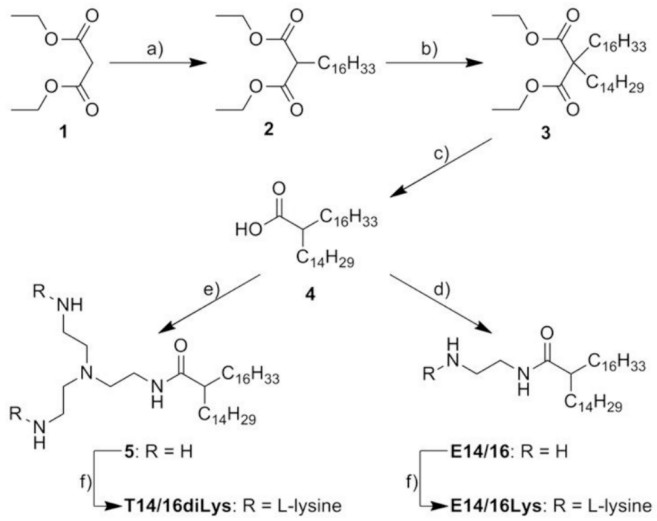

Scheme 1. Synthesis of the three ionizable lipids based on 2-tetradecyl octadecanoic acid. Synthetic conditions: a) NaH, hexadecyl bromide, toluene, reflux; b) NaH, tetradecyl bromide, xylene, reflux; c) 1. NaOH, ethanol, reflux; 2. HCl, water; 3. 200 °C; d) ethylene diamine, triethylamine, PyBOP, methylene chloride, room temperature; e) tris(2-aminoethyl)amine, triethylamine, PyBOP, methylene chloride, room temperature; f) 1. diBOC-lysine-*N*-hydroxysuccinimide, triethylamine, methylene chloride, room temperature; 2. trifluor acetic acid, methylene chloride, room temperature; 3.·NH_3, water, room temperature. Synthesized compounds: 1) diethyl malonate; 2) 2-hexadecyl diethyl malonate; 3) 2,2-hexadecyl tetradecyl diethyl malonate; 4) 2-tetradecyloctadecanoic acid; 5) 2-tetradecyloctadecanoic acid-[2-bis(2-aminoethyl)aminoethyl]amide.

α-branched fatty acid, namely 2-tetradecyl-octadecanoic acid, as lipophilic part (Fig. 1). The fatty acid was coupled with 3 different head-group moieties resulting in a systematic increase of the volume and the number of primary amino groups (1 NH_2 for **E14/16**, 2 NH_2 for **E14/16Lys**, and 4 NH_2 for **T14/16diLys**). We further studied the monolayer phase behavior of the three ionizable lipids using Langmuir microbalance combined with grazing incidence X-ray diffraction (GIXD). To study the nucleic acid binding capacity of the ionizable lipids, their monolayer properties at the air–water interface in presence and absence of model DNA in the subphase have been investigated using Langmuir microbalance combined with IRRAS. Further, the evaluation of the transfection performance of the novel lipids was performed in cell culture models.

2. Materials and methods

2.1. Synthesis

General. Lipids **E14/16**, **E14/16Lys** and **T14/16diLys** (structures shown in Fig. 1) have been synthesized as shown in Scheme 1 and described below. All chemicals were purchased from Merck KGaA (Darmstadt, Germany) unless stated otherwise. The solvents were analytically pure and dried before use. Thin layer chromatography (TLC), used to check the purity of all compounds, was carried out on aluminum sheets coated with silica gel 60 F254 (Merck). Bromothymol blue spray was used to visualize lipophilic compounds. Column chromatography was performed using silica gel 60 (0.063–0.200 mm) for the normal pressure procedure and silica gel 60 (0.04–0.063 mm) for medium pressure liquid chromatography (MPLC). MPLC was from Büchi (Essen, Germany). The melting points were assigned with a Boetius apparatus representing uncorrected values. For the elemental analyses a CHNS-932 apparatus of the LECO-corporation (St Joseph, Michigan, USA) was used. The ESI-mass spectra were recorded with a Finnigan MAT 719 (Thermo Separation Products, San José, USA) with an electron spray ionization energy of 4.5 kV in negative and positive modus. EI-mass spectra were prepared with an AMD 402 apparatus (70 eV, AMD Intecta GmbH, Harpstedt, Germany). For high resolution mass spectrometry a LTQ-Orbitrap-mass spectrometer (Thermo Fisher Scientific, Bremen, Germany) was used. The ^{1}H NMR and ^{13}C NMR spectra were recorded on Varian Gemini 2000 or a Varian Inova 500 with $CDCl_3$ as internal standard.

*Synthesis of 2-hexadecyl malonic acid diethylester (**2**)*: The monoalkyl malonic acid diethylester was prepared according to literature [18] and purified by column chromatography. Briefly, 1 equivalent sodium hydride (60 % m/m in paraffin) was stirred in toluene and 1 equivalent diethylmalonate were added dropwise while stirring to yield the sodium salt. After visual gas evolution stopped, the mixture was heated to 50 °C for 2 h. Afterwards, 1.15 equivalent hexadecyl bromide was added dropwise while stirring and the mixture was stirred under reflux for 5 h. After dropwise addition of 5 mL water at 0 °C, the organic layer was washed three times with brine, and afterwards organic solvent was removed. The crude product was purified by column chromatography with heptane/diethyl ether gradient technique with increasing polarity.

The analytical data were in agreement with the literature [18].

*Hexadecyltetradecyl malonic acid diethylester **(3)**:* The second alkylation was carried out according to literature [19,20]. 1 equivalent hexadecyl malonic acid diethylester in xylene was added dropwise to 1 equivalent sodium hydride (60 % m/m in paraffin) in xylene while stirring. After the sodium salt has been built (clear solution) 1.15 equivalent tetradecyl bromide was added and the mixture was heated for 10 h under reflux. After dropwise addition of 5 mL water at 0 °C the organic layer was washed three times with brine and the product was purified using column chromatography with heptane/diethyl ether gradient technique.

Yield (87 %) colorless oil, EI-MS (*m/z*): 580 (4 %, [M]); 535 (6 %, [M–C_2H_6O]); 384 (51 %, [M–$C_{14}H_{29}$]); 356 (54 %, [M–$C_{16}H_{32}$]). ^{1}H NMR (400 MHz, $CDCl_3$): δ = 0.85 (6H, t, ^{3}J(H,H) = 6.6 Hz, 2 [H_3C–(CH_2)$_2$-]); 1.17–1.29 (58H, m, [H_3C–(CH_2)$_{12}$-CH_2–], [H_3C–(CH_2)$_{14}$-CH_2–] and 2 [H_3C-CH_2-O-]); 1.81–1.85 (4H, m, [-(CO)$_2$C–(CH_2)$_2$-]); 4.14 (4H, q, ^{3}J(H,H) = 7.1 Hz, 2 [H_3C-CH_2-O-]) ppm. Anal. calcd. for $C_{37}H_{72}O_4$: C, 76.49; H, 12.49; found: C, 76.49; H, 13.02.

2.1.1. 2-tetradecyl octadecanoic acid **(4)**

Compound 3 was saponificated with five equivalents of potassium hydroxide in ethanol (95 % v/v) while stirring for 12 h under reflux. Afterwards the ethanol was evaporated and the residue suspended in water. The acidification with hydrochloric acid yields the alkylated malonic acid which was extracted with chloroform. For decarboxylation the dried product was heated for 30 min to 200 °C. The product was purified by recrystallization from heptane.

Yield (46 %) white crystalline, mp: 62 °C EI-MS (*m/z*): 480 [100 %, M]; 284 [56 %, M–$C_{14}H_{28}$]; 256 [59 %, M–$C_{16}H_{32}$]. ^{1}H NMR (400 MHz, $CDCl_3$): δ = 0.85 (6H, t, ^{3}J(H,H) = 6.6 Hz, 2 [H_3C–(CH_2)$_2$-]); 1.17–1.60 (56H, m, [H_3C–(CH_2)$_{13}$-] and [H_3C–(CH_2)$_{15}$-]);2,21–2,29 (1H, m, [–C*H*-COOH]) ppm. Anal. calcd. for $C_{37}H_{72}O_4$: C, 76.49; H, 12.49; found: C, 76.49; H, 13.02.

*2-Tetradecyl octadecanoic acid (2-aminoethyl)amide **E14/16**:* 5 mmol tetradecyloctadecanoic acid, 5 mmol (2.6 g) benzotriazol-1-yloxytripyrrolidinophosphonium hexafluorophosphate (PyBOP) and 5 μL trimethylamine (TEA) dissolved in 100 mL methylene chloride were dropped into 100 mmol ethylene diamine with stirring. The mixture was stirred for further 12 h at room temperature and afterwards washed three times with water. After drying over sodium sulfate the solvent was evaporated. The crude product was purified by MPLC with chloroform/methanol/NH_3 with increasing polarity.

Yield: (42 %), ESI-MS (*m/z*): 524.2 [M + H]$^+$. ^{1}H NMR (500 MHz, $CDCl_3$): δ = 0.87 (6H, t, ^{3}J(H,H) = 6.9 Hz, 2[H_3C-CH_2–]); 1.24–1.61 (56H, m, [H_3C–(CH_2)$_{13}$-] and [H_3C–(CH_2)$_{15}$-]); 2.00–2.09 (m, 1H, [–C*H*-CO-]); 2.01 (t, 2H, ^{3}J(H,H) = 5.6 Hz [H_2N-CH_2–]); 3.45–3.49 (m, 2H, [H_2N-CH_2-CH_2-NHCO]), 6.44–6.48 (m, 1H, [–CON*H*-]) ppm. ^{13}C NMR (125 MHz, $CDCl_3$): δ = 14.1, 22.7, 27.7, 29.4, 29.56, 29.57, 29.66, 29.69, 29.71, 29.75, 31.92, 32.88, 32.99, 39.9, 41.2, 47.8, 177.4 ppm. Anal. Calcd. for $C_{34}H_{70}N_2O$: C, 78.09; H, 13.49; N, 5.36; found: C, 78.14; H, 13.10; N, 5.11.

2.1.2. 2-Tetradecyl octadecanoic acid [2-(2,6-diamino-1-oxohexyl) aminoethyl]amid **E14/16Lys**

3 mmol of **E14/16** was dissolved in 10 mL methylene chloride. 1 mmol of diBOC-lysine-*N*-hydroxysuccinimide and 1 mmol TEA were added with stirring. The mixture was stirred for 12 h at room temperature and subsequently evaporated. For BOC-cleavage the crude compound was suspended in 10 mL ethyl acetate and 5 drops hydrochloric acid (36 % m/m in water) were added. The mixture was stirred for 2 h. After that the solvent was evaporated and the product purified by MPLC with chloroforme/methanol/ammonia with gradient technique

Yield: 57 %, white waxy substance, HR-MS calcd. for $C_{40}H_{83}N_4O_2$: 651.6511. Found: 651.6504. ^{1}H NMR (500 MHz, $CDCl_3$): δ = 0.87 (6H, t, ^{3}J(H,H) = 6.9 Hz, 2[H_3C–]); 1.24–1.90 (62H, m, [H_3C–(CH_2)$_{13}$-], [H_3C–(CH_2)$_{15}$-] [H2N-CH_2–(CH_2)$_3$ –CH–]); 2.10–2.14 (1H, m, [–CO-C*H*(CH_2)$_2$-]); 3.05–3.07 (2H, m, [H_2N-CH_2–]); 3.30–3.36 (4H, m, 2[–HN-(CH_2)$_2$-]); 3.86–3.88 (1H, m, [NH_2-C*H*-CO–]); 7.40–7.44 (m, 1H, [–CON*H*-]); 7.50–8.53 (m, 1H, [–CON*H*-]) ppm. ^{13}C NMR (125 MHz, $CDCl_3$): δ = 14.1, 22.0, 22.7, 26.8, 27.6, 29.4, 29.6, 29.7, 29.8, 32.0, 32.7, 39.0, 39.2, 39.6, 47.3, 53.8, 172.8, 177.4 ppm.

2.1.3. 2-tetradecyloctadecanoic acid-{2-bis[(2,6-diamino-1-oxohexyl) aminoethyl]aminoethyl} amide **T14/16diLys**

2-Tetradecyloctadecanoic acid (1 mmol) and 1 mmol PyBOP and 5 μL trimethylamine (TEA) dissolved in 100 mL methylene chloride were added dropwise to tris(2-aminoethyl)amine (200 mmol) while stirring. The yielded crude compound 5 was purified by MPLC with chloroform/methanol/NH_3 with increasing polarity. Afterwards, the coupling of two equivalents diBOC-lysine-*N*-hydroxysuccinimide using the protocol described for the synthesis of **E14/16Lys** yields **T14/16diLys**. The crude product was purified by MPLC with chloroform/methanol/ammonia with gradient technique.

Yield: 35 %, white waxy substance, HR-MS calcd. for $C_{50}H_{105}N_8O_3$: 865.8305. Found: 865.8304. ^{1}H NMR (500 MHz, $CDCl_3$): δ = 0.87 (6H, t, ^{3}J(H,H) = 6.9 Hz, 2[H_3C–]); 1.23–1.82 (68H, m, [H_3C–(CH_2)$_{13}$-], [H_3C–(CH_2)$_{15}$-] 2[H2N-CH_2–(CH_2)$_3$ –CH–]); 2.08–2.10 (1H, m, [–CO-C*H*(CH_2)$_2$-]); 2.53–2.62 (6H, m, [–CH_2-N(–CH_2–)$_2$]); 2.69–2.74 (4H, m, 2 [H_2N-CH_2–]); 3.24–3.36 (8H, m, 3[–HN-(CH_2)$_2$-] and 2[NH_2-C*H*-CO–]); 6.70–6.74 (m, 1H, [–CON*H*-]); 7.67–7.69 (m, 2H, 2[–CON*H*-]) ppm. ^{13}C NMR (125 MHz, $CDCl_3$): δ = 14.8, 22.7, 23.1, 27.8, 29.3, 29.63, 29.69, 29.8, 31.9, 32.8, 33.0, 34.9, 37.5, 37.6, 41.6, 47.5, 54.7, 55.2, 175.4, 176.5 ppm.

2.2. Physical-chemical characterization methods

General. For all monolayer experiments, 1 mM solutions of each ionizable lipid in chloroform were used. The corresponding solution was spread onto the subphase with a microsyringe and left for 10 min to assure complete chloroform evaporation. For experiments with DNA, 0.1 mM solution of calf thymus DNA (ctDNA) in MiliQ water was used as subphase. For DNA adsorption, the lipid monolayer was incubated for 1 h at the water/air interface before starting compression.

Film Balance Measurements. The surface pressure/area (π/A) isotherms were measured using a computer-interfaced Langmuir trough (R&K, Potsdam, Germany) equipped with a Wilhelmy balance for surface tension measurements. The films spread on an aqueous subphase were compressed at a rate of 5 Å^{2}molecule^{-1}min^{-1}. The temperature of the subphase was kept constant for each measurement with an accuracy of 0.1 °C.

Infrared Reflection-Absorption Spectroscopy (IRRAS). The method was described previously [16]. Briefly, infrared reflection–absorption spectra were recorded on a Vertex 70 FT-IR spectrometer (Bruker, Ettlingen, Germany) equipped with a Mercury Cadmium Telluride (MCT) detector cooled with liquid nitrogen and attached to an external air/water reflection unit (XA-511 Bruker). The IR beam was polarized by KRS-5 wire grid polarizer in the plane of incidence (p) and perpendicular to this plane (s). Spectra were recorded with a resolution of 8 cm^{-1} and scanning velocity of 20 kHz. The angle of incidence normal to the surface Φ was 40° for all measurement. The setup consisted of two Langmuir troughs: one with the investigated monolayer spread on a subphase (sample trough), the second one filled with the corresponding pure subphase (reference trough), allowing sample and reference spectra recording within a short time by a shuttling technique to minimize interferences from carbon dioxide and water vapor from the beam path. The whole setup was placed into a closed plexiglass chamber to maintain a constant humidity. The reflectance-absorbance was calculated using –log(R/R_0), with R being the reflectance of the sample trough and R_0 the reflectance of the reference trough. The lipid phase state under given compression was checked by the position (peak maximum) of the asymmetric CH_2-stretching vibration band. The quantification of DNA attached to the lipid monolayer was performed

using the area of the asymmetric and symmetric phosphate stretching vibration bands of the DNA backbone. The p/s dichroic ratio for DNA backbone was calculated to check if the polarization of light influences signal intensity. Briefly, intensity quotient (I p-polarized IR beam /I s-polarized IR beam) was calculated for the respective band. Exact procedure was described elsewhere [16]. No dependence has been found and spectra obtained with s-polarized light were used for further analysis. To determine the amount of DNA per lipid molecule, the number of lipid molecules in IRRAS footprint (the illuminated area was ~ 2 mm^2) has been calculated using the area per lipid molecule at a given surface pressure from the corresponding π/A isotherm, and the quotient of the intensity of phosphate bands and the calculated number of lipid molecules in the IR footprint was calculated for each measured surface pressure. For calculation of the charge density of the theoretically fully protonated lipids at a given surface pressure, the number of primary amines in one ionizable lipid molecule (z) was divided by the molecular area determined at a given surface pressure from the corresponding π/A isotherm of the lipid (A in $Å^2$).

Grazing Incidence X-Ray Diffraction (GIXD). All measurements were performed on the liquid surface diffractometer (undulator beamline BW1) at HASYLAB, DESY, Hamburg, Germany. The Langmuir trough was located in the temperature controlled, hermetically closed container flushed with helium. A beryllium (0 0 2) crystal has been used to yield a monochromatic beam with a wavelength (λ) of 1.304 Å. The incidence angle at the liquid surface was set to 0.11° (~85 % of the critical angle for total external reflection for water). A linear position-sensitive detector (OED-70-M, Braun, Garching, Germany) was used to record the intensity of the diffracted beam as a function of the vertical scattering vector [$Q_z = (2\pi/\lambda)\sin\alpha_f$] and horizontal scattering vector [$Q_{xy} = (4\pi/\lambda)\sin(2\theta/2)$], where α_f is the vertical and 2θ is the horizontal scattering angle. The horizontal resolution (0.008 A^{-1}) was determined by a Soller collimator (JJ X-RAY, Denmark) located between the sample and the detector. The intensities were corrected for polarization, effective area, and Lorentz factor. The diffraction data consist of Bragg peaks in the 2-dimensional Q_{xy}/Q_z space. Model peaks taken as Lorentzian in the in-plane direction (Bragg peak Q_{xy}) and as Gaussian in the out-of-plane direction (Bragg rod Q_z) were fitted to the background corrected intensities using Origin software. The in-plane lattice repeat distances of the ordered structures then follow from Bragg's law: repeat distance = $2\pi/Q_{xy}$. The tilt of the chains with respect to the vertical direction is obtained from the Q_z positions of the peaks.[21,22] The Q_{xy} and Q_z values were used to calculate lattice unit cell parameters, unit cell distortion (d), chain tilt angle (t) and chain cross-section area (A_0). The correlation length L_{xy} can be determined with Scherrer formula $L_{xy} = 0.88(2\pi/\Delta Q_{xy})$ where ΔQ_{xy} is the full-width at half-maximum of the Lorenzian peak corrected with the detector resolution. The length of the scattering unit (length of a single chain) can be calculated using $L_z = 0.88(2\pi/\Delta Q_z)$, with ΔQ_z being the full-width at half-maximum of the Gaussian peak.

Dynamic Light Scattering and Laser Doppler Anemometry. Particle size as z-average diameter and ζ-potential were measured via dynamic light scattering (DLS) and laser Doppler anemometry, respectively, using a Zetasizer Nano-ZS (Malvern-Panalytical, UK). For measurements, 20 μL of the liposome dispersion (c = 1 mg/mL) were diluted to 1 mL with water and transferred into a cuvette with 10 mm path length for DLS and afterwards in a U-folded capillary cell for ζ-potential measurement. DLS and ζ potential measurements were performed at 25 °C, while 3 measurements consisting of 10 runs were performed. DLS was measured with automated attenuation and laser position. The assumed refractive index of the measurement parameters was 1.330. The z-average diameter d was calculated from the determined diffusion coefficient D using Stokes-Einstein law with $d = (kT)/(3\pi\eta D)$ where k is the Boltzmann-constant, T is the temperature, and η the viscosity taken as 0.8872 mPa s. The calculated polydispersity index (PDI) gives information of the size distribution range. ζ potential was calculated from the electrophoretic mobility μ using Smoluchowsky law $\mu=(\varepsilon\zeta)/\eta$, where ε is the dielectric constant and η the viscosity. The voltage of 50 V was used for measurement and η = 0.8872 mPa s and ε = 78.5 F/m were used for calculation. All calculations were made using the Zetasizer Software 6.34.

2.3. Biological experiments

Preparation of Liposomes. A 2 mg/mL solution of the ionizable lipid in $CHCl_3$/methanol (1/1, v/v) was combined with 1 mg/mL solution of 1,2-di-(*9Z*-octadecenoyl)-*sn*-glycero-3-phosphoethanolamine (DOPE) in $CHCl_3$/methanol (1/1, v/v) to achieve a molar ionizable lipid/DOPE ratio of 1/2 ($n_{ionizable\ lipid}/n_{DOPE}$). The mixtures were dried under reduced pressure at 37 °C to remove the organic solvent, and the dried film was vacuum-desiccated for 2 h. The lipid film was dispersed in sterile filtered water (membrane filter pore size 220 nm) at room temperature to a final concentration of 1 $mg_{total\ lipid}$/mL, and incubated in a water bath at 37 °C for at least 15 min for film hydration. Subsequently, the lipid formulations were vortexed and treated in a bath sonicator (2–3 cycles of 15 min at 37 °C) until an opalescent liposome dispersion was obtained. The samples were stored in the refrigerator at 4 °C before use.

Preparation of Plasmid DNA. pCMV Sport β-Gal plasmid was produced in *Escherichia coli* DH5α (Invitrogene life technologies) and isolated using a Quiagen plasmid mega kit (Quiagen) following the manufacturer's instructions. DNA with an OD_{260}/OD_{280} (OD = optical density) between 1.8 and 2 was used for experiments. The absence of genomic DNA was proved by agarose gel electrophoresis analysis.

Cell Culture. Hep-G2 cells (human hepatocytes) were cultured in 75 cm^2 tissue culture flasks in MEM medium adjusted to contain 2 mM glutamine, 0.05 mg/mL gentamycin 10 mM MEM non-essential amino acids, 1 mM sodium pyruvate and 10 % fetal bovine serum (FBS) at 37 °C and 5 % CO_2. The cells were grown confluent and were regularly split twice a week. Only cells between passage 5 and 40 were used for transfection and MTT experiments.

Transfection Biology. Cells were seeded into a 96 well plate with 200 μL cell suspension per well at a density of 1 10^5 to 1.2 10^5 cells per mL and cultured for 16 to 24 h. Lipoplex mixtures were prepared by combining plasmid DNA (0.15 μg per well) with varying amounts of cationic liposome suspension to obtain different N/P ratios (ratio of the numbers of primary amino groups in ionizable lipids to the number of phosphate groups in the DNA) with FBS-free MEM as dispersion medium. The lipoplex samples were incubated for 15 min at room temperature before adding them to cells. Cells were washed once with phosphate buffered saline (PBS) and 40 μL FBS-free lipoplex solution was added to each well for 4 h of incubation. Afterwards, 60 μL cell culture medium with 10 % FBS was added to each well. The total medium was refreshed after 24 h by medium with 10 % FBS.

Reporter gene activity was determined 48 h post transfection. Therefore, the cells were washed with PBS lysed for 15 min in lysis buffer (5 mM Chaps in 50 mM Hepes buffer) ant centrifuged to obtain the lysis supernatant. 60 μL supernatant were given in the wells of a 96 well plate and 60 μL substrate solution [1.33 mg/mL of *O*-nitrophenyl-*β-D*-galactopyranoside (ONPG), $MgCl_2$ 2 mM, mercaptoethanol 100 mM in 0.2 M sodium phosphate pH 7.3] were added per well and the assay was incubated for 30 min at 37 °C. The reaction was stopped with 1 M sodium carbonate aqueous solution. Absorption at 405 nm was converted to *β*-galactosidase units using a calibration curve obtained from commercial *β*-galactosidase enzyme. *β*-galactosidase was normalized to the protein content. Protein concentration was quantified with bichinonic acid reaction [23]. Absorption at 570 nm was converted into protein concentration by using a calibration curve made of bovine serum albumin.

Toxicity Assay. Cytotoxicity of the lipoplexes was assessed by the 3-(4,5-dimethylthiazol-2-yl)-2,5-diphenyltetrazolium bromide (MTT) assay. The cytotoxicity assays were performed in 96 well plates by maintaining the same ratio and number of cells and lipoplexes as used in the transfection experiments. MTT was added after refreshing the

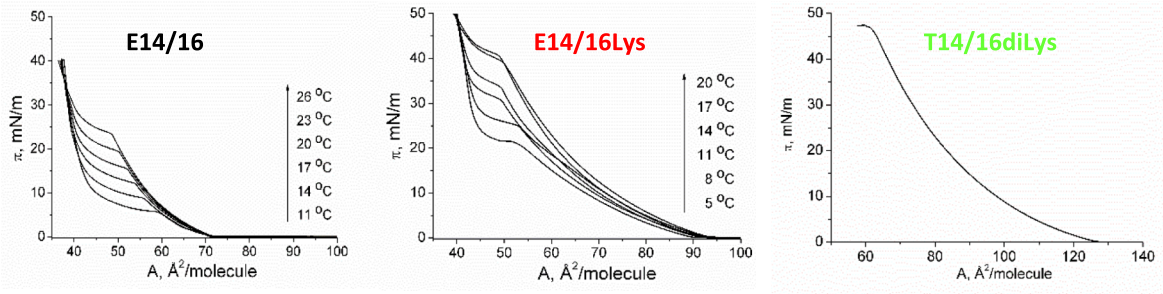

Fig. 2. Surface pressure (π) – area (A) isotherms of **E14/16** (left) and **E14/16Lys** (middle) at different temperatures on a water subphase at pH 5.5. The isotherm of **T14/16diLys** (right) was taken at 20 °C.

medium (24 h after addition of lipoplexes to the cells) and incubated for 3 h at 37 °C. Afterward, the cells were lysed with a mixture of 10 % sodium dodecyl sulfate in acetic acid/dimethyl sulfoxide. The resulting formazan was quantified at 570 nm. The results were expressed as percent viability: [A570 (lipoplex treated cells) − background]/[A570 (untreated cells) − background] × 100 %.

Statistical analysis. Data of multiple measurements are given as mean average and standard deviation. Statistical testing of transfection efficiency was done with Kruskal Wallis testing followed by Dunńs Bonferoni post-hoc test using GraphPad Prism software.

3. Results and discussion

3.1. Synthesis of ionizable lipids based on branched fatty acids

The synthesis (Scheme 1) of the new branched fatty acid amides starts from diethyl malonate (**1**) using a strategy described earlier [23]. The modular synthesis strategy allows a stepwise structural modification of new compounds. The hexadecyl malonic acid diethyl ester (**2**) was synthesized by alkylation of diethyl malonate (**1**) with hexadecyl bromide. The precursor (**2**) was transformed into dialkyl malonic acid diester (**3**) by a second alkylation with tetradecyl bromide [24]. After saponification and decarboxylation, the branched fatty acid (**4**) was available for the assembly of the head-group structure. Using PyBOP mediated coupling of ethylene diamine, a reaction commonly used in peptide synthesis, **E14/16** was synthesized. The lipid **E14/16Lys** was built by coupling one lysine molecule to the head-group of **E14/16**. The amide was formed by treating **E14/16** with the activated ester diBOC-lysine-*N*-hydroxysuccinimide, followed by cleavage of the BOC protective group using trifluor acetic acid. The lipid **T14/16diLys** is characterized by a branching in the head-group region which was achieved by coupling tris(2-aminoethyl)amine to the branched fatty acid (**4**). The two primary amino groups of the lipid intermediate (**5**) could react with diBOC-lysine-*N*-hydroxysuccinimide, and after BOC-cleavage with TFA the ionizable lipid **T14/16diLys** was yielded.

Consequently, we had a series of three ionizable lipids with identical lipophilic part and directed variation in head-group size. **E14/16** has a small head-group of an ethylamine residue. **E14/16Lys** is characterized by a lysine head-group, with two primary amines. **T14/16diLys** is the lipid with the largest head-group consisting of two separated lysine moieties with consequently four primary amino functions, and an additional tertiary amine from the tris(aminoethyl)amine branching. Although the pKa of primary amino functions of molecules in solution ranges between 8 and 10, the apparent pKa values in lipid associates can range between 6 and 4 [14]. Hence, the real protonation degree of the lipids at given pH cannot be estimated solely by the structure and number of amines in the head-group.

3.2. Structural information of the ionizable lipids from analysis of Langmuir monolayers

First, the monolayer structures of the ionizable lipids have been evaluated before studying the interaction with the nucleic acid. The system was kept as simple as possible by using deionized water saturated with CO_2 leading to a pH of 5.5. This allowed us to avoid effects on the monolayer structure resulting from ions of buffer substances, and also effects of buffer ions, e.g. phosphate, on IRRA spectra.

The π/A isotherms of the 3 lipids are presented in Fig. 2. **T14/16diLys** remains in the liquid expanded (LE) phase state, with high mobility of the alkyl chains (*gauche* conformation of fluid alkyl chains), up to the collapse pressure of ~ 45 mN/m (Fig. 2, right). **E14/16** and **E14/16Lys** show a first-order phase transition (plateau region) from LE to liquid condensed (LC) phase (Fig. 2, left and middle), which allows us to perform thermodynamic calculations. The LC phase is characterized by ordered alkyl chain packing (alkyl chain in *all-trans* conformation). For **E14/16**, a second-order phase transition can be seen characterized by a kink in the isotherm (change of the slope between 30 and 35 mN/m, Fig. 2, left). The kink indicates the transition from the tilted to the non-

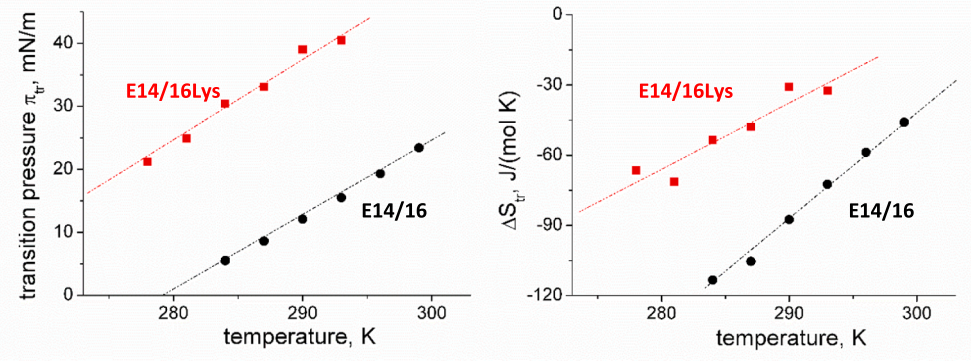

Fig. 3. Transition pressure (π_{tr}) and entropy change (ΔS) of **E14/16** (●) and **E14/16Lys** (■) on a water subphase as a function of temperature and their linear fits (dotted lines).

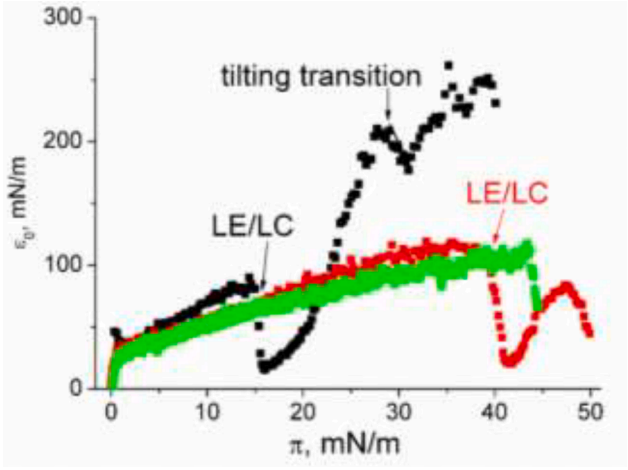

Fig. 4. Surface compression modulus ε_0 of **E14/16** (■), **E14/16Lys** (■) and **T14/16diLys** (■) monolayers on a water subphase at 20 °C.

tilted state of ordered alkyl chains.

Thermodynamic analysis (see explanation in supporting information) allows determining characteristic temperatures (Fig. 3). T_0 is the temperature minimum for the existence of the LE phase. For **E14/16**, T_0 = 279.7 K (6.5 °C), and for **E14/16Lys**, T_0 = 262.1 K (−11.1 °C) were determined. The second temperature is the critical temperature (T_c). Above T_c, the LC state cannot be reached by further compression and the phase transition vanishes. For **E14/16**, T_c = 308.7 K (35.5 °C) and for **E14/16Lys**, T_c = 303.3 K (30.1 °C) were determined. For **E14/16Lys**, both temperatures are lower than the corresponding temperatures of **E14/16**. These differences are an effect of the bigger size of the **E14/16Lys** head-group which reduces the ability of carbon chains to interact and align.

Using *eq. (3)*, the surface compression modulus, ε_0, the value defining monolayers capacity for energy storage, was calculated for the three lipids at 20 °C (Fig. 4) [25–27]:

$$\varepsilon_0 = -A(d\pi/dA) \quad (3)$$

with A as the molecular area at a given surface pressure and $d\pi/dA$ as the slope of the isotherm at this area A.

At 20 °C, both **E14/16** and **E14/16Lys** monolayers undergo the first-order phase transition, while the monolayer of **T14/16diLys** remains fluid up to the collapse, as already seen in the isotherms in Fig. 2. Fig. 4 shows that monolayers of all lipids have very similar elastic properties in the LE phase, and the values are comparable with those reported for dioleoylphosphatidyl choline [28]. For **E14/16** and **E14/16Lys**, elasticity drops at the phase transition pressure and then rises again when the lipids organize in the LC phase [29]. In case of **E14/16**, a second local minimum around 30 mN/m can be observed, assigned to the already mentioned second-order phase transition to the untilted state. Comparison of elastic properties of **E14/16** and **E14/16Lys** in the LC phase is difficult, since the monolayer of **E14/16Lys** collapses shortly after the phase transition. Consequently, elasticity was also calculated for **E14/16** and **E14/16Lys** monolayers at lower temperatures (11 and 14 °C) (supporting information, Figure S1). It is clearly seen that the **E14/16** monolayer is more elastic than **E14/16Lys**. This observation indicates a stiff hydrogen bonding network in the head-group region of **E14/16Lys** between amino and carbonyl groups (see also GIXD experiments) what makes the monolayer less resistant to stress.

GIXD is a powerful tool to study chain packing of lipids in monolayers in LC phases. X-ray diffraction pattern gives information about dimensions of chain lattice unit cell, its distortion (d), tilt angle of chains (t) and cross-sectional area of chains (A_0) [30]. **E14/16** and **E14/16Lys** were studied at different (indicated) surface pressures in the LC state on the water subphase at 10 and 5 °C, respectively. **T14/16diLys** does not form a LC phase under analyzed conditions. Fig. 5 shows selected contour plots from GIXD intensities as a function of the in-plane (Q_{xy}) and the out-of-plane (Q_z) scattering vector components at various surface pressures. Maxima of Q_{xy} and Q_z peaks, values of d, t, A_0 and correlation lengths (L_{xy} and L_z) of both lipids are summarized in the supporting information Table S2. The contour plot of **E14/16Lys** at 20 mN/m exhibits four well-resolved peaks. Two are assigned to the alkyl chain lattice: one at Q_z = 0.41 Å^{-1} (degenerated peak, dg, Fig. 5) and the other one at Q_z = 0.82 Å^{-1} (non-degenerated peak, non-dg, Fig. 5) indicating the chain packing in a centered rectangular lattice distorted towards next-nearest neighbor (NNN) with NNN-tilted chains [31]. With increasing surface pressure, the distance between both peaks decreases, and both peaks move in the direction of smaller Q_z values, indicating a decrease of lipid chain tilt angle and unit cell distortion. Up to surface pressures of 40 mN/m, no transition into the hexagonal phase with non-tilted chains can be observed. This is in good agreement with the estimated value (based on the analysis of the tilt angle: 1/cos(t) vs. π, see SI) of the phase transition from the tilted to the untilted state ($\pi_{t'}$ = 78.2 mN/m), a surface pressure much above the collapse pressure. The peak at the same Q_{xy} value as the non-degenerated one is an effect of signal intensity modulation and does not correspond to any structure. The peak at Q_{xy} = 1.3 Å^{-1} (d = 4.83 Å) is characteristic for a lattice resulting from hydrogen bonds which can be formed between the lipid head-groups (peak H-bond Fig. 5). A comparable hydrogen bond network is known from other lipids with lysine in the head-group [16].

Even though **E14/16** head-groups also have moieties that can form hydrogen bonds (primary amines, amides), the hydrogen bond peak was not observed in GIXD. The contour plot of **E14/16** at lower surface pressures (13 mN/m) presents two resolved peaks, one located at Q_z = 0 Å^{-1} (non-degenerated peak, non-dg label Fig. 5) while the second can be observed at higher Q_z and lower Q_{xy} values (degenerated peak, dg label, Fig. 5). Such positions of peaks are characteristic for a distorted towards nearest neighbor (NN) centered rectangular chain lattice with NN-tilted chains [31]. Upon further compression, the degenerated peak moves to smaller Q_z values what indicates decrease of aliphatic chains tilt and unit cell distortion. At 30 mN/m, the peaks are still slightly resolved, whereas at 40 mN/m their positions coincide giving one well-defined peak at Q_z = 0 Å^{-1}, which corresponds to the non-distorted hexagonal lattice with untilted chains. The determined (by 1/cos(t) vs. π, see supporting information) surface pressure of the transition from the tilted to untilted state ($\pi_{t'}$ = 32.6 mN/m) is in good agreement with the presented contour plots.

Additional information can be obtained from IRRAS on Langmuir monolayers. Recording IRRA spectra enables the direct determination of a change of the phase state in the monolayer by position of CH_2 symmetric, ν_s (CH_2), and asymmetric, ν_{as} (CH_2), stretching vibrations. In the LE phase, these bands are around 2853 cm^{-1} and 2924 cm^{-1}, respectively, while for LC they are shifted to lower wavenumbers around 2849 cm^{-1} and 2919 cm^{-1} [32–34], respectively. Representative spectra showing the shift of both bands during lipid monolayer compression resulting in the LE/LC phase transition are presented in Figure S3 (supporting information). The positions of the ν_{as} (CH_2) stretching band are plotted in dependence of π for the three investigated lipids on water (Fig. 6, left).

For **E14/16**, the characteristic position shift of ν_{as} (CH_2) from ~ 2924 cm^{-1} to ~ 2919 cm^{-1} indicating the LE/LC phase transition can be clearly seen. The conformation of chains changes between surface pressure of 15 and 21 mN/m, what is in a good agreement with the phase transition pressure observed in the π/A isotherm by a plateau (15.5 mN/m, T = 20 °C). **E14/16Lys** shows also the LE/LC phase transition between 30 and 40 mN/m in good agreement with the corresponding π/A isotherm (~40 mN/m), nevertheless, the drop of the wavenumber is less sharp compared to **E14/16**. The monolayer of **T14/16diLys** is fluid with wavenumbers between 2926 and 2925 cm^{-1} in the whole range of measured surface pressures (0 – 40 mN/m).

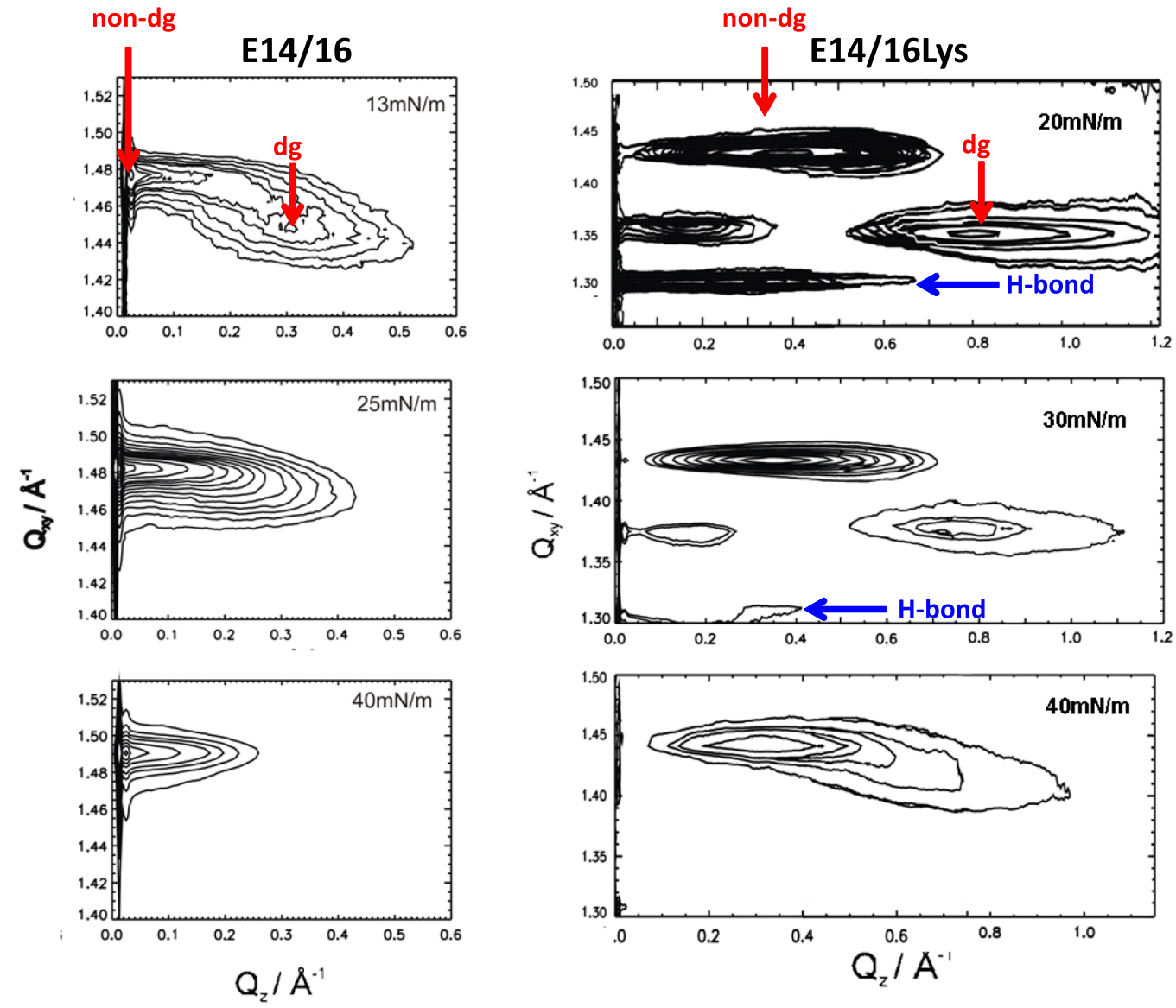

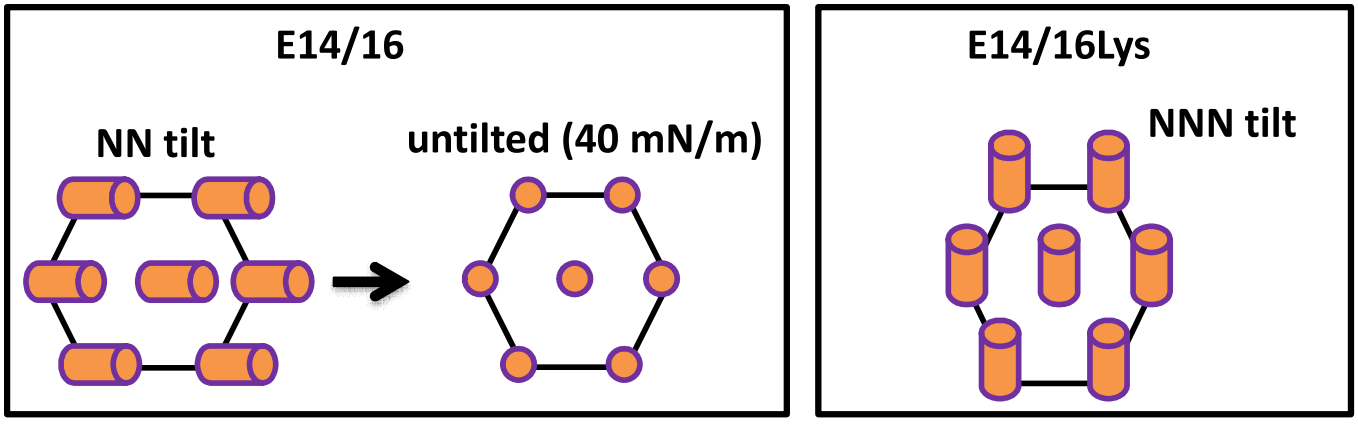

Fig. 5. Contour plots of GIXD intensities as a function of the in-plane scattering vector component Q_{xy} and the out-of-plane scattering vector component Q_z of monolayers of lipids spread on water: **E14/16** at 10 °C (at 13, 25 and 40 mN/m) and **E14/16Lys** at 5 °C (at 20, 30 and 40 mN/m). The peaks assigned to the chain lattice are labelled with non-dg for the non-degenerated and dg for the degenerated peak. The peak resulting from the hydrogen bond lattice is labelled with H-bond. The illustration below explains the found alkyl chain lattices. **E14/16** (left): centered rectangular lattice distorted towards nearest neighbor (NN) with the NN-tilted chains and non-distorted hexagonal with untilted chains at high surface pressure; **E14/16Lys** (right): centered rectangular lattice distorted towards next-nearest neighbor (NNN) with NNN-tilted chains.

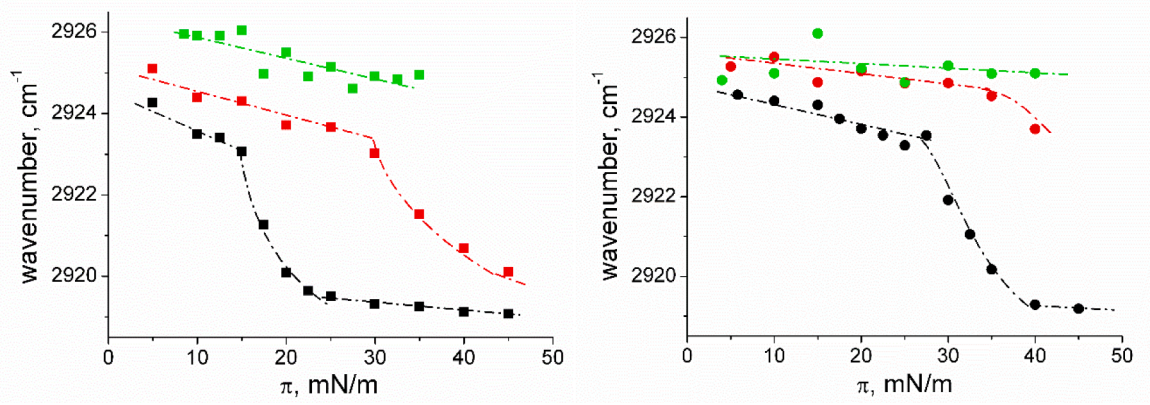

Fig. 6. The positions of ν_{as} (CH_2) band of **E14/16** (■), **E14/16Lys** (■) and **T14/16diLys** (■) on water (left) and on 0.1 mM ctDNA aqueous solution (right) along the compression isotherm at 20 °C measured by IRRAS. The dotted lines are a guide for the eye.

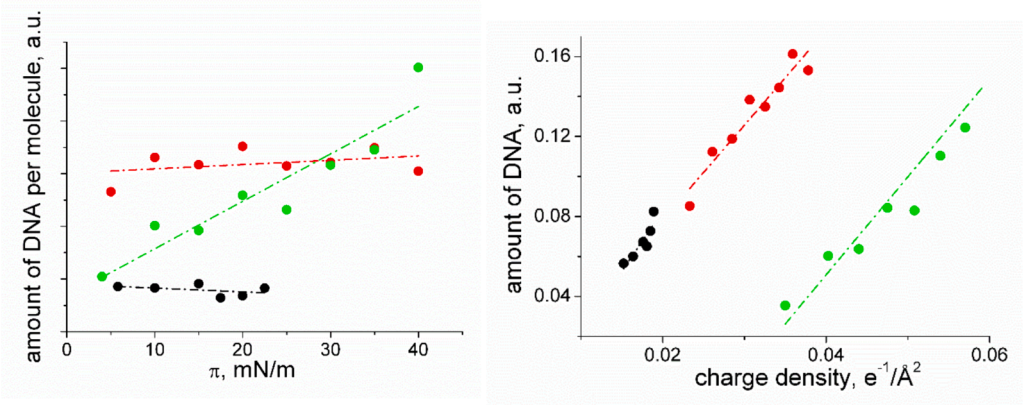

Fig. 7. (left) Relative amount of DNA per lipid molecule bound to **E14/16** (●), **E14/16Lys** (■) and **T14/16diLys** (●) monolayers spread on 0.1 mM ctDNA aqueous solution determined by IRRAS via integration of the ν_s (PO_2) and ν_{as} (PO_2) peaks resulting from the phosphate groups in the DNA backbone. (right) Relative amount of DNA plotted as the function of the charge density in the lipid monolayer.

3.3. *The effect of DNA binding to the ionizable lipids*

IRRAS allows studying the interaction of nucleic acids with the novel ionizable lipids, since DNA is the only compound that has phosphate groups in this experimental setup. The relative amount of DNA attached to the monolayer can be calculated by determination of the intensity of typical symmetric, ν_s (PO_2), and asymmetric, ν_{as} (PO_2), phosphate diester bands at around 1082 cm^{-1} and 1238 cm^{-1}, respectively. DNA can be also detected by presence of the DNA backbone band at 970 cm^{-1} [15,35–37].

Before quantifying the amount of DNA binding capacity, the effect of bound DNA on the phase behavior has been checked by IRRAS examining the ν_{as} (CH_2) band (Fig. 6, right). For **E14/16** on DNA subphase, the LE/LC phase transition of the lipid is shifted to much higher surface pressures (between 30 and 40 mN/m) compared to the DNA-free subphase. A partial incorporation of bound DNA into the fluid **E14/16** monolayer at low surface pressure can explain this behavior, since the lipid is spread on the DNA solution. However, the positions of the ν_{as} (CH_2) band of **E14/16** on water and DNA are the same above the phase transition, what indicates that DNA is squeezed out from the LC monolayer at higher surface pressures, and the lipid packing density is the same as on water. For **E14/16Lys**, the attached negatively charged DNA strands drastically increase the disorder of the lipid chains in the monolayer. No LE/LC transition can be detected, contrary to the lipid on water in absence of DNA. **T14/16diLys** remained in the LE phase also in presence of DNA with ν_{as} (CH_2) values comparable to those on pure water. Summarizing, binding of nucleic acids to the three ionizable lipids has a fluidizing effect.

The amount of DNA bound to the lipid monolayers was quantified at different surface pressures during the monolayer compression using IRRAS (supporting information Figure S4). The interpretation of the data needs further normalization, because the number of molecules in the infrared footprint area (constant illuminated area) of the monolayer is different, due to the different lipid packing densities. Therefore, the relative amount of DNA bound to one lipid molecule at a given surface pressure in the LE phase was calculated (Fig. 7, left). **E14/16** and **E14/16Lys** showed a constant DNA binding capacity in the LE phase, while **T14/16diLys** shows a surface pressure dependent binding. Moreover, approximately two times more DNA is attached to **E14/16Lys** than to **E14/16** what could be expected since **E14/16Lys** has twice as many primary amines. The situation is different for **T14/16diLys**, where the amount of DNA increases linearly with surface pressure (Fig. 7, left), to reach values equal or even higher than for **E14/16Lys** at surface pressures above 30mN/m. This can be explained by a surface pressure dependent change in protonation degree and/or conformational accessibility of the amine groups of **T14/16diLys** for DNA complexation. Different protonation degrees for different surface pressures of the same monolayer have been observed before, but usually the number of charges decreases with increasing packing density of the monolayer [38]. However, the theoretically expected value of twice as much DNA as bound to **E14/16Lys** is not reached (2 NH_2 for **E14/16Lys** vs. 4 NH_2 for **T14/16diLys**). This is supported by the plot of the amount of bound DNA against the theoretical charge density of the lipids with fully protonated primary amines (Fig. 7, right). Although the theoretical charge

Table 1
Z-average diameter (d),polydispersity index (PDI), and ζ-potential of the liposomes composed from the ionizable lipids in water. The given values represent mean ± standart deviation (s) of three measurements.

lipid composition	d (z-average) ± s [nm]	PDI ± s	ζ-potential ± s [mV]
E14/16:DOPE 1:2 (n:n)	178 ± 4	0.32 ± 0.01	45 ± 2
E14/16Lys:DOPE 1:2 (n:n)	106 ± 2	0.42 ± 0.02	31 ± 2
T14/16diLys:DOPE 1:2 (n:n)	82 ± 14	0.34 ± 0.08	56 ± 5

density of **T14/16diLys** is much higher, the amount of bound DNA is pronounced lower compared to **E14/16Lys** at the same theoretical charge density. Steric effects can explain this observation, meaning that the area per head-group is not big enough to fit higher amounts of DNA, or the conformation of the head-group of **T14/16diLys** is unfavorable.

3.4. Gene transfer efficacy

For initial efficacy testing, a feasible lipoplex formation approach, well established in our lab [23], was used. The ionizable lipids were mixed with DOPE in a molar ratio of 1/2 (n/n) and formulated to cationic liposomes, which are capable to complex nucleic acids due to the positively charged character. Particle size and charge of the liposomes, which were used for nucleic acid complexation in the transfection experiments, have been determined (see Table 1). The observed differences between the lipid compositions were not pronounced. The particle size slightly decreases with increasing head-group size (from 178 nm to 82 nm). The polydispersity index (PDI) of all lipid compositions indicates a polydisperse system with a broader size distribution, what was expected because no extrusion was performed during liposome preparation. All lipid compositions are positively charged with ζ-potential values between 31 mV and 56 mV, indicating a positive surface charge. The gene transfer activities and cytotoxicity of lipid formulations with different N/P ratios were screened in a Hep-G2 cell culture model (Fig. 8). For this purpose a constant dose of DNA, encoding for the β-galactosidase reporter gene, was complexed with different amounts of the liposomes composed of the ionizable lipid/DOPE 1/2 (n/n) composite. The reporter gene (vector: p-CMV-SPORT-β-Gal) results in an expression of β-galactosidase after successful gene transfer, and transfection efficiency correlates with the β-galactosidase activity [39]. The cell viability was determined by MTT-assay [40].

Correlations between structure and transfection efficiency can be seen. The transfection efficiency increases with increasing head-group size and increasing number of primary amines with **T14/16diLys** as the most effective lipid. For instance, **T14/16diLys** formulations at an N/P ratio of 1.5 and 2.5 showed significant higher β-galactosidase activity compared to 3 of the 4 tested **E14/16** formulations (Fig. 8). Further, all tested **T14/16diLys** formulations and **E14/16Lys** formulations at N/P ratio of 1, 1.5 and 2 show a trend of higher efficacy compared with Lipofectamine^{TM} lipofection standard (see Fig. 8).

3.5. Summarizing discussion

We were able to synthesize three ionizable lipids using an optimized synthesis strategy to systematically vary the lipid structure. For instance, divalent and trivalent amines could successfully couple to the carboxyl group without protective groups to avoid byproducts caused by multiple amide formation using a high excess of tris(2-amonoethyl)amine and ethylene diamine, respectively. The synthesized ionizable lipids are characterized by an increasing head-group size and increasing number of amino groups. This has the effect, that in the sequence **E14/16** < **E14/16Lys** < **T14/16diLys** the packing parameter P decreases (Fig. 9). P is calculated as V/(A·L), where V is the volume of the alkyl chains, A is

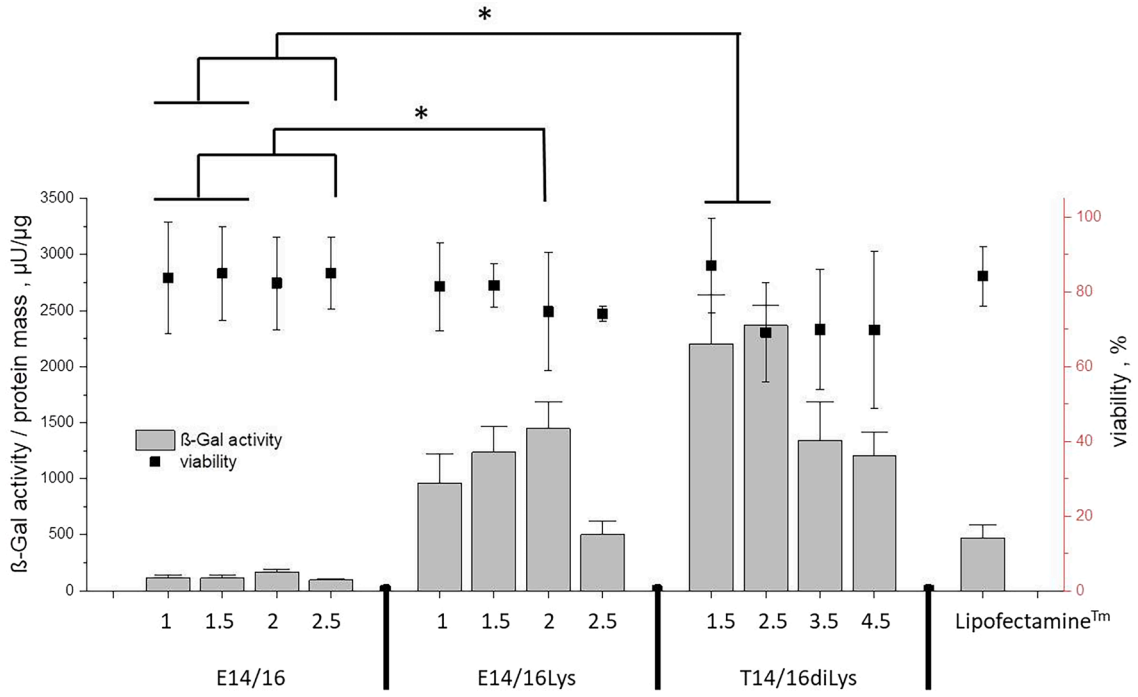

Fig. 8. Results of the transfection efficiency as ß-galactosidase activity normalized to total protein content and the cell viability values of the ionizable lipids **E14/16**, **E14/16Lys**, and **T14/16diLys** in mixture with the co-lipid DOPE in ratio of 1/2 ($n_{ionizable}$ lipid/n_{DOPE}) compared to Lipofectamine® reagent in Hep-G2 cells. The values show the mean ± standard deviation (n ≥ 3). The numbers given for the ionizable lipid represent the N/P ratio, defined as molar ratio of primary amino functionalities of the ionizable lipids to the phosphate functions in the DNA. With a constant plasmid concentration of 0.1 µg per well, the dose of lipids increases with increasing N/P ratio. Significance was tested using Kruskal Wallis analysis with post-hoc Dunn's Bonferonis test with an α value of 0.05. Significant differences with $p \leq 0.05$ are labelled with *.

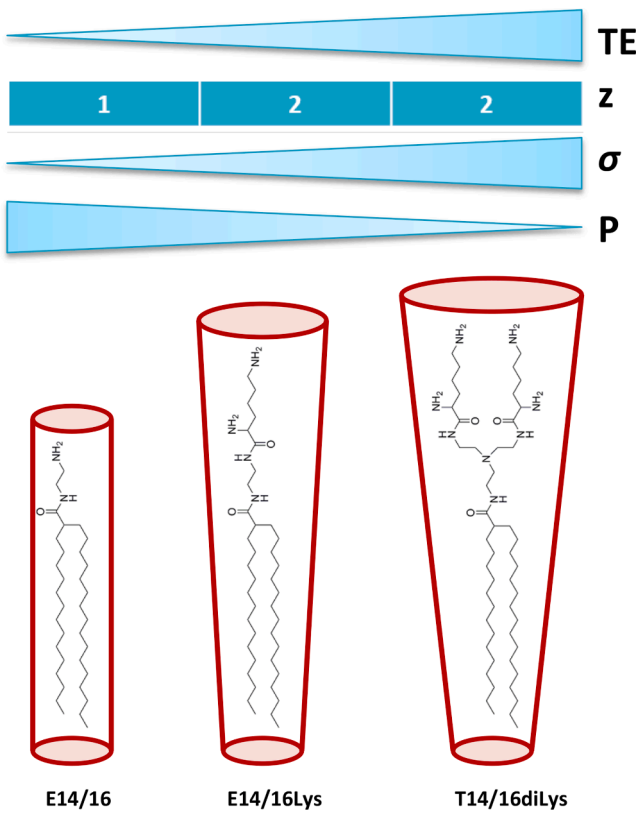

Fig. 9. Summary of this study. From **E14/16** → **E14/16Lys** → **T14/16diLys**, the packing parameter P decreases, while charge density σ and transfection efficiency TE increase. The effective DNA binding groups z do not correspond to the number of primary amines.

the area of the hydrophilic head-group, and L the length of the alkyl chain part [41]. Because of the comparable lipophilic part, V and L can be assumed as equal and the decreasing P value results from the increasing head-group size and consequently increasing A. This has different effects for the ionizable lipids. With decreasing P value, starting from P≈1, a higher curvature in the self-assembled structures of amphiphiles can be assumed. Hence, the assembly of **E14/16Lys** or **T14/16diLys** into cubic or hexagonal structures is a possible scenario, but needs to be investigated by small-angle x-ray scattering. The decreasing packing parameter has further effects, hence, the interaction of the lipid alkyl chains in self-assembled structures decreases. As consequence, T_c decreases (**E14/16** > **E14/16Lys**, **T14/16diLys** was in the LE state) while the head-group increases. T_c is comparable with the main phase transition temperature in lipid bilayers, if the geometrical packing of lipids in monolayer and bilayer is comparable [16,42]. In bilayer experiments we could confirm the increasing phase transition temperature for the sequence **E14/16** > **E14/16Lys**, **T14/16diLys** via differential scanning calorimetry (see Figure S5 and chapter 3 in the SI). Nevertheless, the values for the phase transition differed from the determined T_c values, This observation indicates different packing properties between monolayer and bilayer, e.g. differences in the head group hydrogen bond networks [16] or interdigitation of alkyl chains in lipid bilayers [43]. Also IRRAS demonstrated that fluidity of the lipid monolayer increases with increasing head-group size and charge (higher values of the $-CH_2$ stretching vibration wavenumbers). The same applies to the LE/LC phase transition. For lipids with smaller head-groups, effective alkyl chain contact is realized; hence, phase transition for **E14/16** occurs at lower surface pressures than for **E14/16Lys**. In case of **T14/16diLys**, it is impossible to reduce the size of the head-group by surface pressure so much to allow effective alkyl chain interactions. The increasing alkyl chain fluidity seems to be connected with an increased transfection efficacy, since **T14/16diLys** was the most effective lipid (Fig. 8).

However, alkyl chain fluidity is not the only aspect which has to be discussed. Charge density is another crucial parameter, because it affects the strength of nucleic acid binding [15]. In the present case, the charge density of the lipids increases with increasing number of primary amines. Nevertheless, also steric aspects have to be taken into account. The DNA binding studies demonstrated that **T14/16diLys** had at least comparable binding capacities to **E14/16Lys**, even though the number of primary amino groups was twice as much as in **E14/16Lys**. Nevertheless, the efficacy screening demonstrated highest efficiency for **T14/16diLys**, showing that binding capacity is not the dominating parameter for the transfection efficacy (TE). Binding affinity is also a key parameter. The DNA binding studies demonstrated that **E14/16** and **E14/16Lys** bound the same amount of DNA per lipid independent of the surface pressure, while for **T14/16diLys** the bound amount of DNA per lipid molecule was a function of the surface pressure. We assume that the binding affinity of **T14/16diLys** to DNA changes while changing the surface pressure. This affects DNA binding and encapsulation. If the binding affinity also decreases during transfer of DNA-lipid nanoparticles from endosome to cytosol, an effective release can be assumed. This hypothesis has to be addressed in ongoing research.

To address the complexity of lipid formulation development, a more detailed understanding in lipid mixing behaviour is necessary which exceeds the scope of this article. While herein preliminary transfection data were obtained from ionizable lipid/DOPE 1/2 (n/n), additional screening of mixtures with varying ionizable lipid/DOPE molar ratios and other co-lipids, e.g. cholesterol or 1,2-dioleoyl-*sn*-glycero-3-phosphocholine, are required to be addressed in future research on the novel lipids. These lipid mixtures need to be investigated regarding the nucleic acid encapsulation efficiency using gel electrophoretic screening of uncomplexed nucleic acid and ethidium bromide exclusion assay of the lipid formulation at different N/P ratios [15]. Additionally, small angle x-ray scattering experiments are needed to understand the lipid self assembly in bulk and the structural aspects of complex formation between lipids and nucleic acids [44,45]. Such information is needed to derive further structure activity relationships. Finally, the type of nucleic acid can be varied, e.g. small interfering RNA or mRNA instead of DNA.

4. Conclusion

The three newly synthesized lipids designed for gene transfection, **E14/16**, **E14/16Lys** and **T14/16diLys** were investigated in order to improve knowledge of transfection efficiency/lipid structure correlation. In this study, their monolayer properties at the air–water interface have been investigated using the Langmuir trough in combination with IRRAS and GIXD. The two-dimensional binding of these monolayers with model DNA dissolved in the water subphase has been also investigated by quantifying the amount of DNA attached to a monolayer using IRRAS. All lipids show different structures and affinity to DNA due to different size and charge of the head-group. With increasing head-group size, the alkyl chain fluidity increases. With increasing number of primary amines in the head-group, the charge density of lipid assemblies increases, resulting in increased nucleic acid binding. Nevertheless, steric effects control the accessibility of DNA binding functions in these lipids. Also the nucleic acid binding affinity can be tuned with the head-group structure. From the investigated lipids, **T14/16diLys** was the most effective one in preliminary in vitro screening. Ongoing research will focus on nanoparticle formulation studies and more detailed efficacy screenings.

CRediT authorship contribution statement

Dorota Pawlowska: Writing – original draft, Investigation, Funding acquisition, Formal analysis. **Nicole Erdmann:** Investigation, Formal

analysis. **Manuela Folz:** Investigation, Formal analysis. **Andreas Langner:** Supervision, Resources. **Bodo Dobner:** Writing – review & editing, Supervision, Resources, Conceptualization. **Christian Wölk:** Writing – review & editing, Writing – original draft, Supervision, Formal analysis. **Gerald Brezesinski:** Writing – review & editing, Supervision, Funding acquisition, Conceptualization.

Declaration of competing interest

The authors declare that they have no known competing financial interests or personal relationships that could have appeared to influence the work reported in this paper.

Data availability

Data will be made available on request.

Acknowledgement

We thank HASYLAB at DESY, Hamburg, Germany, for beamtime at the DORIS beamline BW1 and excellent support. This work has been supported by the Max Planck Society and by the European Union in the framework of European Social Fund through the Warsaw University of Technology Development Program, realized by the Centre for Advanced Studies.

Appendix A. Supplementary data

Supplementary data to this article can be found online at https://doi.org/10.1016/j.ejpb.2024.114338.

References

[1] G. Ferrari, A.J. Thrasher, A. Aiuti, Gene therapy using haematopoietic stem and progenitor cells, Nat. Rev. Genet. 22 (2021) 216–234.
[2] M. Friedrich, A. Aigner, Therapeutic siRNA: State-of-the-Art and Future Perspectives, BioDrugs 36 (2022) 549–571.
[3] A. Akinc, M.A. Maier, M. Manoharan, K. Fitzgerald, M. Jayaraman, S. Barros, S. Ansell, X. Du, M.J. Hope, T.D. Madden, B.L. Mui, S.C. Semple, Y.K. Tam, M. Ciufolini, D. Witzigmann, J.A. Kulkarni, R. van der Meel, P.R. Cullis, The Onpattro story and the clinical translation of nanomedicines containing nucleic acid-based drugs, Nat. Nanotechnol. 14 (2019) 1084–1087.
[4] R. Verbeke, I. Lentacker, S.C. de Smedt, H. Dewitte, The dawn of mRNA vaccines: The COVID-19 case, J. Control. Release 333 (2021) 511–520.
[5] X. Wang, S. Liu, Y. Sun, X. Yu, S.M. Lee, Q. Cheng, T. Wei, J. Gong, J. Robinson, X. Di Zhang, P. Lian, D.J.S. Basak, Preparation of selective organ-targeting (SORT) lipid nanoparticles (LNPs) using multiple technical methods for tissue-specific mRNA delivery, Nat. Protoc. 18 (2023) 265–291.
[6] L. Schoenmaker, D. Witzigmann, J.A. Kulkarni, R. Verbeke, G. Kersten, W. Jiskoot, D.J. Crommelin, mRNA-lipid nanoparticle COVID-19 vaccines: Structure and stability, Int. J. Pharm. 601 (2021) 120586.
[7] Q. Cheng, T. Wei, L. Farbiak, L.T. Johnson, S.A. Dilliard, D.J. Siegwart, Selective organ targeting (SORT) nanoparticles for tissue-specific mRNA delivery and CRISPR–Cas gene editing, Nat. Nanotechnol. 15 (2020) 313–320.
[8] C. Stefaniu, G. Brezesinski, Grazing incidence X-ray diffraction studies of condensed double-chain phospholipid monolayers formed at the soft air/water interface, Adv. Colloid Interface Sci. 207 (2014) 265–279.
[9] C. Stefaniu, G. Brezesinski, H. Möhwald, Langmuir monolayers as models to study processes at membrane surfaces, Adv. Colloid Interface Sci. 208 (2014) 197–213.
[10] C. Stefaniu, G. Brezesinski, X-ray investigation of monolayers formed at the soft air/water interface, Curr. Opin. Colloid Interface Sci. 19 (2014) 216–227.
[11] I.S. Zuhorn, V. Oberle, W.H. Visser, J.B. Engberts, U. Bakowsky, E. Polushkin, D. Hoekstra, Phase behavior of cationic amphiphiles and their mixtures with helper lipid influences lipoplex shape, DNA translocation, and transfection efficiency, Biophys. J. 83 (2002) 2096–2108.
[12] V. Oberle, U. Bakowsky, I.S. Zuhorn, D. Hoekstra, Lipoplex formation under equilibrium conditions reveals a three-step mechanism, Biophys. J . 79 (2000) 1447–1454.
[13] M.N. Antipina, B. Dobner, O.V. Konovalov, V.L. Shapovalov, G. Brezesinski, Investigation of the protonation state of novel cationic lipids designed for gene transfection, J. Phys. Chem. B 111 (2007) 13845–13850.
[14] S. Tassler, C. Wölk, C. Janich, B. Dobner, G. Brezesinski, Lysine-based amino-functionalized lipids for gene transfection: the protonation state in monolayers at the air–liquid interface, PCCP 19 (2017) 20271–20280.
[15] C. Janich, C. Wölk, F. Erdmann, T. Groth, G. Brezesinski, B. Dobner, A. Langner, Composites of malonic acid diamides and phospholipids — Impact of lipoplex stability on transfection efficiency, J. Control. Release 220 (2015) 295–307.
[16] M. Dittrich, M. Böttcher, J.S.L. Oliveira, B. Dobner, H. Möhwald, G. Brezesinski, Physical–chemical characterization of novel cationic transfection lipids and the binding of model DNA at the air–water interface, Soft Matter 7 (2011) 10162–10173.
[17] S. Tassler, D. Pawlowska, C. Janich, B. Dobner, C. Wölk, G. Brezesinski, Lysine-based amino-functionalized lipids for gene transfection: the influence of the chain composition on 2D properties, PCCP 20 (2018) 6936–6944.
[18] R.R. Schmidt, K. Jankowski, New types of nonionic surfactants with sugar head groups, Liebigs Ann./recl. 1996 (1996) 867–879.
[19] V.G. Bier, Über die Viskosität von Verzweigten verbindungen, Makromol. Chem. 4 (1949) 124–133.
[20] V.H. Staudinger, G. Bier, G. Lorentz, Viskositätsuntersuchungen an niedermolekularen estern mit verzweigten molekülen, Makromol. Chem. 3 (1949) 251–280.
[21] J. Als-Nielsen, D. Jacquemain, K. Kjaer, F. Leveiller, M. Lahav, L. Leiserowitz, Principles and applications of grazing incidence X-ray and neutron scattering from ordered molecular monolayers at the air-water interface, Phys. Rep. 246 (1994) 251–313.
[22] C. Stefaniu, C. Wölk, G. Brezesinski, E. Schneck, Relationship between structure and molecular interactions in monolayers of specially designed aminolipids, Nanoscale Adv. 1 (2019) 3529–3536.
[23] N. Erdmann, C. Wölk, I. Schulze, C. Janich, M. Folz, S. Drescher, M. Dittrich, A. Meister, J. Vogel, T. Groth, B. Dobner, A. Langner, Tris(2-aminoethyl)amine-based α-branched fatty acid amides – Synthesis of lipids and comparative study of transfection efficiency of their lipid formulations, Eur. J. Pharm. Biopharm. 96 (2015) 349–362.
[24] F.L. Breusch, E. Ulusey, Synthese der d, l-Di-n-alkyl-essigsäuren mit 19 bis 23 C-Atomen. (VI. Mitteil. über isomere und homologe Reihen), Chem. Ber. 86 (1953) 688–692.
[25] N. Sakamoto, K. Sakai, K. Takagi, Measurements of surface elasticity and thickness of ${4}^{\ensuremath{'}}\ensuremath{-}n$-octyl-4-cyanobiphenyl film at an air-water interface, Phys. Rev. E 56 (1997) 1838–1843.
[26] I. López-Montero, L.R. Arriaga, G. Rivas, M. Vélez, F. Monroy, Lipid domains and mechanical plasticity of Escherichia coli lipid monolayers, Chem. Phys. Lipids 163 (2010) 56–63.
[27] A. Lucero, M.R. Rodríguez Niño, A.P. Gunning, V.J. Morris, P.J. Wilde, J. M. Rodríguez Patino, Effect of hydrocarbon chain and pH on structural and topographical characteristics of phospholipid monolayers, J. Phys. Chem. B 112 (2008) 7651–7661.
[28] M.R.R. Niño, A.L. Caro, J.M.R. Patino, Structural, topographical, and rheological characteristics of β-casein–dioleoyl phosphatidylcholine (DOPC) mixed monolayers, Colloids Surf. B Biointerfaces 69 (2009) 15–25.
[29] E.A. Montanha, F.J. Pavinatto, L. Caseli, O. Kaczmarek, J. Liebscher, D. Huster, O. N. Oliveira, Properties of lipophilic nucleoside monolayers at the air–water interface, Colloids Surf. B Biointerfaces 77 (2010) 161–165.
[30] T.R. Jensen, K. Kjaer, Structural Properties and Interactions of Thin Films at the Air-Liquid Interface Explored by Synchrotron X-Ray Scattering, in: D. Möbius, R. Miller (Eds.), Studies in Interface Science Novel Methods to Study Interfacial Layers, Elsevier, 2001, pp. 205–254.
[31] V.M. Kaganer, H. Möhwald, P. Dutta, Structure and phase transitions in Langmuir monolayers, Rev. Mod. Phys. 71 (1999) 779–819.
[32] R. Mendelsohn, G. Mao, C.R. Flach, Infrared reflection–absorption spectroscopy: Principles and applications to lipid–protein interaction in Langmuir films, Biochim. Biophys. Acta Biomembr. 1798 (2010) 788–800.
[33] R. Mendelsohn, J.W. Brauner, A. Gericke, External infrared reflection absorption spectrometry of monolayer films at the air-water interface, Annu. Rev. Phys. Chem. 46 (1995) 305–334.
[34] R.A. Dluhy, D.G. Cornell, In situ measurement of the infrared spectra of insoluble monolayers at the air-water interface, J. Phys. Chem. 89 (1985) 3195–3197.
[35] S.H. Brewer, S.J. Anthireya, S.E. Lappi, D.L. Drapcho, S. Franzen, Detection of DNA hybridization on gold surfaces by polarization modulation infrared reflection absorption spectroscopy, Langmuir 18 (2002) 4460–4464.
[36] Q. Chen, X. Kang, R. Li, X. Du, Y. Shang, H. Liu, Y. Hu, Structure of the complex monolayer of Gemini surfactant and DNA at the air/water interface, Langmuir 28 (2012) 3429–3438.
[37] M. Tsuboi, Application of infrared spectroscopy to structure studies of nucleic acids, Appl. Spectrosc. Rev. 3 (1970) 45–90.
[38] A. Gericke, H. Hühnerfussf, The conformational order and headgroup structure of long-chain alkanoic acid ester monolayers at the air/water interface, Ber. Bunsen. Phys. Chem 99 (1995) 641–650.
[39] A. Lazik, Y. Liu, P. Bringas, F. Sangiorgi, R. Maxson, A sensitive method for analyzing β-galactosidase reporter gene expression in tissue sections of mouse embryos, Trends Genet. 12 (1996) 445–447.
[40] T. Mosmann, Rapid colorimetric assay for cellular growth and survival: Application to proliferation and cytotoxicity assays, J. Immunol. Methods 65 (1983) 55–63.
[41] J.N. Israelachvili, 19 - Thermodynamic Principles of Self-Assembly, in: J. N. Israelachvili (Ed.), Intermolecular and Surface Forces (third Edition), Academic Press, San Diego, 2011, pp. 503–534.
[42] G. Brezesinski, H. Möhwald, Langmuir monolayers to study interactions at model membrane surfaces, Adv. Colloid Interface Sci. 100–102 (2003) 563–584.

[43] A. Zumbuehl, B. Dobner, G. Brezesinski, Phase behavior of selected artificial lipids, Curr. Opin. Colloid Interface Sci. 19 (2014) 17–24.
[44] M. Dittrich, C. Brauer, S.S. Funari, B. Dobner, G. Brezesinski, C. Wölk, Interactions of cationic lipids with DNA: a structural approach, Langmuir 34 (2018) 14858–14868.
[45] S. Tassler, B. Dobner, L. Lampp, R. Ziółkowski, E. Malinowska, C. Wölk, G. Brezesinski, DNA Delivery systems based on peptide-mimicking cationic lipids—the effect of the Co-lipid on the structure and DNA binding capacity, Langmuir 35 (2019) 4613–4625.